Interval Finite Element Analysis of Thin Plates

M. V. Rama Rao[1)], R. L. Muhanna[2)] and R. L. Mullen[3)]
[1)]*Vasavi College of Engineering, Hyderabad - 500 031 India, dr.mvrr@gmail.com*
[2)]*School of Civil and Environmental Engineering, Georgia Institute of Technology Atlanta, GA 30332-0355, USA, rafi.muhanna@gtsav.gatech.edu*
[3)]*School of Civil and Environmental Engineering, University of South Carolina, GA 30332-0355, USA, rlm@cec.sc.edu*

Abstract: This paper focuses on the analysis of thin plates with uncertain structural parameters modelled as intervals. The plate is assumed to be orthotropic. Interval uncertainty is associated with the Young's modulus of the plate and also with the applied load. Interval Finite Element Method (IFEM) developed in the earlier work for line elements of the authors for truss and frame structures (Rama Rao et al., 2011) is applied to the case of thin plates in the present work. This method is capable of obtaining bounds for interval forces and moments with the same level of sharpness as displacements and rotations. Example problems pertaining to various edge conditions of the thin plate are solved to demonstrate that the present method is capable of obtaining sharp bounds. Results are compared to the values of displacements and forces obtained using combinatorial and Monte Carlo solutions.

Keywords: interval, interval finite elements, uncertainty, thin plates, structural analysis

1. Introduction

Plates play a major role in several important structures viz. ships, pressure vessels, and other structural components. Thus it is important to understand their structural behaviour and possible conditions of failure especially under conditions of uncertainty. The structural behaviour of thin plates in bending depends on several important factors including load, stiffness characteristics of plate and support conditions. The problem of plate bending is one of the oldest in the theory of elasticity and is discussed in several textbooks (Timoshenko and Krieger, 1959; Szilard, 2004; Reddy, 2007). Lim et.al. (2007) derived exact analytical solutions to bending of rectangular thin plates by employing the Hamiltonian principle with Legendre's transformation. The solution obtained by them for example problems of plates with selected boundary conditions shows excellent agreement with the classical solutions. Batista (2010) used the Fourier series to compute the analytical solutions of uniformly loaded rectangular thin plates with symmetrical boundary conditions.

On the other hand, structural analysis without considering uncertainty in loading or material properties leads to an incomplete understanding of the structural performance. Structural analysis using interval variables has been used by several researchers to incorporate uncertainty into structural analysis (Koyluoglu, Cakmak and Nielson, 1995; Muhanna and Mullen, 1995; Nakagiri and Yoshikawa, 1996; Rao and Sawyer, 1995; Rao and

Berke, 1997; Rao and Chen, 1998; Muhanna and Mullen, 2001; Pownuk, 2004; Neumaier and Pownuk, 2007).

To the authors' knowledge, applications of interval methods for the analysis of plates with uncertainty of load and material properties do not exist anywhere in literature. In view of this, we present an initial investigation into the application of interval finite element methods to problems of bending of thin plates. Usually, derived quantities in Interval Finite Element Method (IFEM) such as stresses and strains have additional overestimation in comparison with primary quantities such as displacements. This issue has plagued displacement-based IFEM for quite some time. The recent development of mixed/hybrid IFEM formulation by the authors (Rama Rao et al., 2011) is capable of simultaneous calculation of interval strains and displacements with the same accuracy.

This work presents the application of interval finite element methods to the analysis of thin plates. Uncertainty is considered in both the applied load and Young's modulus as explained in section 2. Examples are finally presented and discussed. In the present study a rectangular plate is analysed different type of edge conditions of such as clamped and simply supported edge conditions and the deformations are obtained.

2. Linear Interval Finite Element Method

Finite element method is one of the most common numerical methods for solving differential and partial differential equations with enormous applications in different fields of science and engineering. Interval finite element methods have been developed to handle the analysis of systems for which uncertain parameters are described as intervals. A variety of solution techniques have been developed for IFEM. A comprehensive review of these techniques can be found in (Zhang, 2005; Muhanna et al., 2007; Rama Rao et al., 2011). Interval analysis concerns the numerical computations involving interval numbers. All interval quantities will be introduced in non-italic boldface font. The four elementary operations of real arithmetic, namely addition (+), subtraction (-), multiplication (×) and division (÷) can be extended to intervals. Operations $\circ \in \{+,-,\times,\div\}$ over interval numbers x and y are defined by the general rule (Moore, 1966; Moore, 1979; Moore et al., 2009; Neumaier, 1990)

$$\mathbf{x} \circ \mathbf{y} = [\min(x \circ y), \max(x \circ y)] \quad for \ \circ \in \{+,-,\times,\div\}, \tag{1}$$

in which x and y denote generic elements $x \in$ x and $y \in$ y. Software and hardware support for interval computation are available such as (Sun microsystems, 2002; Knüppel, 1994; INTLAB, 1999). For a real-valued function $f(x_1,...,x_n)$, the interval extension of $f(\,)$ is obtained by replacing each real variable xi by an interval variable xi and each real operation by its corresponding interval arithmetic operation. From the fundamental property of inclusion isotonicity (Moore, 1966), the range of the function $f(x_1,...,x_n)$ can be rigorously bounded by its interval extension function

$$f(\mathbf{x}_1,..,\mathbf{x}_n) \supseteq \{ f(x_1,..,x_n) \mid x_1 \in \mathbf{x}_1,.., x_n \in \mathbf{x}_n \} \tag{2}$$

Eq. (2) indicates that $f(\boldsymbol{x}_1,\ldots,\boldsymbol{x}_n)$ contains the range of $f(x_1,\ldots,x_n)$ for all $x_i \in \boldsymbol{x}_i$. A natural idea to implement interval FEM is to apply the interval extension to the deterministic FE formulation. Unfortunately, such a naïve use of interval analysis in FEM yields meaningless and overly wide results (Muhanna and Mullen, 2001; Dessombz et al., 2001). The reason is that in interval arithmetic each occurrence of an interval variable is treated as a different, independent variable. It is critical to the formulation of the interval FEM that one identifies the dependence between the interval variables and prevents the overestimation of the interval width of the results. In this paper, an element-by-element (EBE) technique is utilized for element assembly (Muhanna and Mullen, 2001; Zhang, 2005). The elements are detached so that there are no connections between elements, avoiding element coupling. The Lagrange multiplier method is then employed to impose constraints to ensure the compatibility. Then a mixed/hybrid formulation is incorporated to simultaneously calculate the interval strains and displacements (Rama Rao, Mullen and Muhanna, 2011). This linear formulation results in the interval linear system of equations that has the following structure:

$$(K + B\boldsymbol{D}A)\boldsymbol{u} = a + F\boldsymbol{b}, \tag{3}$$

with interval quantities in $\boldsymbol{D}$ and $\boldsymbol{b}$ only. The term $(K + B\boldsymbol{D}A)$ represents the interval structural stiffness matrix and the $a + F\,\mathbf{b}$ term, the structural loading. Any interval solver can be used to solve Eq. (3), however, the following iterative scheme that is developed by Neumaier and Pownuk (Neumaier and Pownuk, 2007) is superior for large uncertainty, defining:

$$C := (K + BD_0A)^{-1} \tag{4}$$

where D_0 is chosen in a manner that ensures its invertability (often D_0 is selected as the midpoint of **D**), the solution **u** can be written as:

$$\mathbf{u} = (Ca) + (CF)\mathbf{b} + (CB)\mathbf{d} \tag{5}$$

To obtain a solution with tight interval enclosure we define two auxiliary interval quantities,

$$\begin{aligned} \mathbf{v} &= A\mathbf{u} \\ \mathbf{d} &= (D_0 - \mathbf{D})\mathbf{v}, \end{aligned} \tag{6}$$

which, given an initial estimate for **u**, we iterate as follows:

$$\mathbf{v}^{k+1} = \{ACa) + (ACF)\mathbf{b} + (ACB)\mathbf{d}^k\} \cap \mathbf{v}^k, \quad \mathbf{d}^{k+1} = \{(D_{c0} - \mathbf{D}_c)\mathbf{v}^{k+1} \cap \mathbf{d}^k, \tag{7}$$

until the enclosures converge, from which the desired solution **u** can be obtained in a straightforward manner.

In this paper the above mentioned iterative enclosure has been used for the solution of the linear interval system of Eq. (3). The solution includes displacements, strains, and forces simultaneously with the same high level of accuracy.

3. Finite Element Model of the Plate

Thin plates are characterized by a structure that is bounded by upper and lower surface planes that are separated by a distance h as shown in Figure 1. The x-y coordinate axes are located on the neutral plane of the plate (the "in-plane" directions) and the z-axis is normal to the x-y plane. In the absence of in-plane

loading, the neutral plane is at the midpoint through the thickness. In the present work, it will be assumed that the thickness of plate h is a constant. Consequently, the location of the x-y axes will lie at the mid-surface plane (z=0).

In most plate applications, the external loading includes distributed load normal to the plate (z direction), concentrated loads normal to the plate, or in-plane tensile, bending or shear loads applied to the edge of the plate. Such loading will produce deformations of the plate in the x, y, z coordinate directions which in general can be characterized by displacements $u(x, y, z)$, $v(x, y, z)$ and $w(x, y, z)$ in the x, y and z directions, respectively.

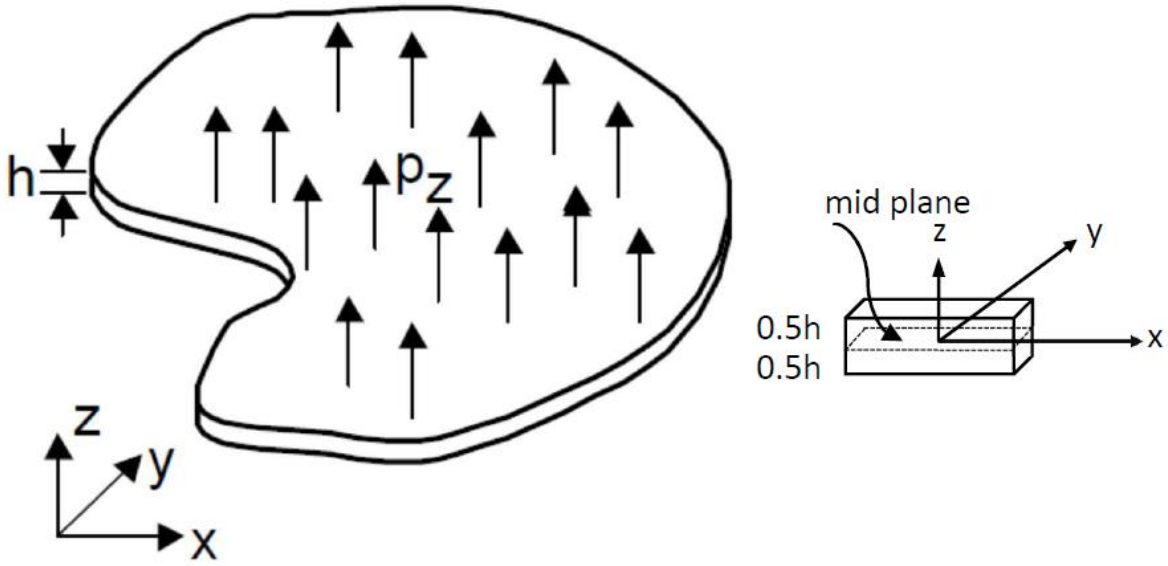

Figure 1. Geometry of thin plate.

The plate is discretized into rectangular ACM (Adini-Clough-Melosh) plate elements. The ACM element is a non-conforming element with 12 degrees of freedom (3 degrees of freedom at each of the four nodes). Degrees of freedom at each node (i) are the transverse displacement and normal rotation about each axis, w_i, $\theta_{xi} = \frac{\partial w_i}{\partial y}$ and $\theta_{yi} = \frac{\partial w_i}{\partial x}$, as illustrated in Figure 2. Note that θ_{yi} is a vector in the *negative* y direction.

Node "1" is selected at the lower left comer of the plate (x=-a, y=-b) and that the nodes are numbered 1,2,3,4 in counterclockwise direction around the plate. We assume that the plate dimensions are given by 2a and 2b as shown in Figure 1 and that the x-y coordinate system is located at the center of plate. The 12 degrees of freedom are arranged in the vector of generalized nodal displacements $\{d\}$ as:

$$\{d\}^T = \{w_1 \quad \theta_{x1} \quad \theta_{y1} \quad w_2 \quad \theta_{x2} \quad \theta_{y2} \quad w_3 \quad \theta_{x3} \quad \theta_{y3} \quad w_4 \quad \theta_{x4} \quad \theta_{y4}\}^T \tag{8}$$

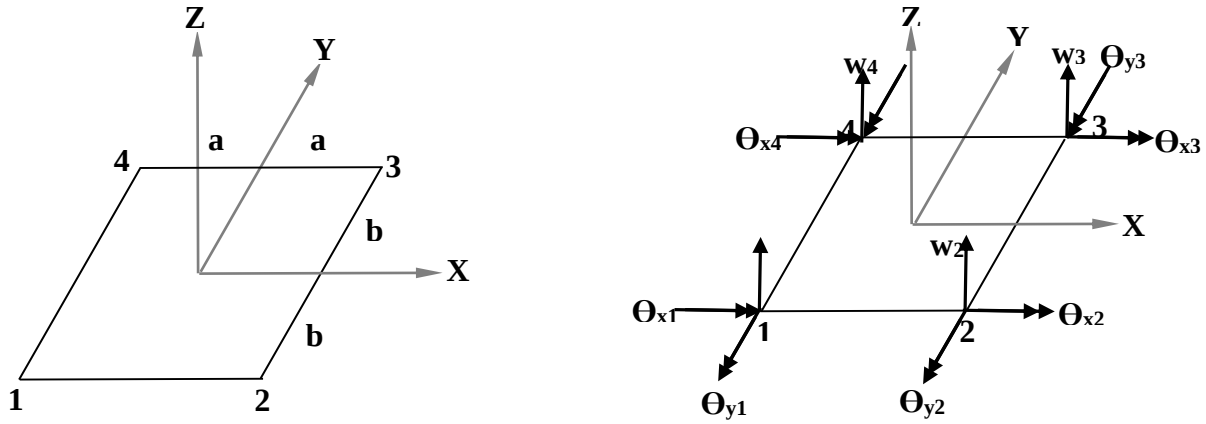

Figure 2. Rectangular element with 12 degrees of freedom.

3.1. STIFFNESS MATRIX AND FORCE VECTOR OF THE ACM PLATE ELEMENT

We assume that $w(x,y)$ is some function over the plate geometry as follows:

$$w(x,y) = a_1 + a_2x + a_3y + a_4x^2 + a_5xy + a_6y^2 + a_7x^3 + a_4x^2y + a_9xy^2 + a_{10}y^3 + a_{11}x^3y + a_{12}xy^3 \quad (9)$$

$$w(x,y) = \begin{bmatrix} 1 & x & y & x^2 & xy & y^2 & x^3 & x^2y & xy^2 & y^3 & x^3y & xy^3 \end{bmatrix} \{\alpha\} \quad (10)$$

which is represented as

$$w(x,y) = \lfloor N(x,y) \rfloor \{\alpha\} \quad (11)$$

$$\begin{Bmatrix} w(x,y) \\ \theta_x \\ \theta_y \end{Bmatrix} = \begin{bmatrix} 1 & x & y & x^2 & xy & y^2 & x^3 & x^2y & xy^2 & y^3 & x^3y & xy^3 \\ 0 & 0 & 1 & 0 & x & 2y & 0 & x^2 & 2xy & 3y^2 & x^3 & 3xy^2 \\ 0 & -1 & 0 & -2x & -y & 0 & -3x^2 & -2xy & -y^2 & 0 & -3x^2y & -y^3 \end{bmatrix} \{\alpha\} \quad (12)$$

Substituting the values of x and y coordinates of nodes 1,2,3,4 of the plate in the Eq. 12 will yield:

$$\{d\} = [\Phi]\{\alpha\} \quad (13)$$

where $\{\alpha\}$ and $\{d\}$ are vector of unknown coefficients and vector of generalized nodal displacements for the element respectively. Substituting $\{\alpha\}$ from Eq. (13) in Eq. (11), we obtain

$$w(x,y) = \lfloor N(x,y) \rfloor [\Phi]^{-1} \{d\} \quad (14)$$

The curvatures of the plate element viz. κ_{xx} , κ_{yy} and κ_{xy} are obtained from the second order partial differentiation of $w(x, y)$ w.r.t x and y as follows:

$$\kappa_{xx} = \frac{\partial^2 w}{\partial x^2} \;\; ; \kappa_{yy} = \frac{\partial^2 w}{\partial x^2} ; \quad \kappa_{xy} = 2\frac{\partial^2 w}{\partial x \partial y} \tag{15}$$

$$\begin{Bmatrix} \kappa_x \\ \kappa_y \\ \kappa_{xy} \end{Bmatrix} = \begin{bmatrix} 0 & 0 & 0 & 2 & 0 & 0 & 6x & 2y & 0 & 0 & 6xy & 0 \\ 0 & 0 & 0 & 0 & 0 & 2 & 0 & 0 & 2x & 6y & 0 & 6xy \\ 0 & 0 & 0 & 0 & 2 & 0 & 0 & 4x & 4y & 0 & 6x^2 & 6y^2 \end{bmatrix} \left[\Phi^{-1}\right]\{d\} \tag{16}$$

Thus the vector of curvatures $\{\kappa^{(e)}\}$ for the plate element can be expressed as

$$\{\kappa^{(e)}\} = \begin{Bmatrix} \kappa_x \\ \kappa_y \\ \kappa_{xy} \end{Bmatrix} = [B][\Phi]^{-1}\{d\} \tag{17}$$

From the moment-curvature relationship $\{M\} = [D]\{\kappa\}$ we obtain

$$\begin{Bmatrix} M_x \\ M_y \\ M_{xy} \end{Bmatrix} = [D]\begin{Bmatrix} \kappa_x \\ \kappa_y \\ \kappa_{xy} \end{Bmatrix} = [D][B][\Phi]^{-1}\{d\} \tag{18}$$

where $[D] = \dfrac{Eh^3}{12(1-\nu^2)} \begin{bmatrix} 1 & \nu & 0 \\ \nu & 1 & 0 \\ 0 & 0 & \dfrac{(1-\nu)}{2} \end{bmatrix}$ (19)

Total potential energy stored in the plate due to bending is given by (Gallagher, 1975; Bathe, 1996)

$$\Pi = \frac{1}{2}\int_{-a}^{a}\int_{-b}^{b} \{\kappa\}^T \{M\} dxdy - \{d\}^T \{P^{(e)}\} = \frac{1}{2}\{d\}^T \left[\Phi^{-1}\right]^T \left(\int_{-a}^{a}\int_{-b}^{b} [B]^T [D][B] dxdy \right) \left[\Phi^{-1}\right]\{d\} - \{d\}^T \{P^{(e)}\} \tag{20}$$

Using the first variation of Π , we obtain,

$$\{P^{(e)}\} = \left[\Phi^{-1}\right]^T \left(\int_{-a}^{a}\int_{-b}^{b} [B]^T [D][B] dxdy \right) \left[\Phi^{-1}\right]\{d\} = [K^{(e)}]\{d\} \tag{21}$$

where the stiffness matrix $[K^{(e)}]$ is given as

$$[K^{(e)}] = \left[\Phi^{-1}\right]^T \left(\int_{-a}^{a}\int_{-b}^{b} [B]^T [D][B] dxdy \right) \left[\Phi^{-1}\right] \tag{22}$$

and the nodal force vector for the plate element $\{P^{(e)}\}$ is given as:

$$\{P^{(e)}\} = [\Phi^{-1}]^T \left(\int_{-a}^{a} \int_{-b}^{b} p_z \lfloor N(x,y) \rfloor^T dxdy \right) \tag{23}$$

4. Interval Finite Element Model of the Plate

An element-by-element (EBE) technique is utilized for element assembly as outlined in section 2. Interval uncertainty is considered in pressure $\boldsymbol{p_z}$ and Young's modulus of the plate $\boldsymbol{E}$. Accordingly, the stiffness matrix and the force vector of the plate element are rewritten, denoting interval quantities in boldface, as follows:

$$[\boldsymbol{K}^{(e)}] = \int_{-a}^{a} \int_{-b}^{b} [B\Phi^{-1}]^T [\boldsymbol{D}] [B\Phi^{-1}] dxdy \tag{24}$$

and

$$\{\boldsymbol{P}^{(e)}\} = [\Phi^{-1}]^T \left(\int_{-a}^{a} \int_{-b}^{b} \boldsymbol{p}_z [N(x,y)]^T dxdy \right) \tag{25}$$

For convenience, $[B\Phi^{-1}]$ is denoted as $[B_1]$. Thus Equation (24) can be rewritten as

$$[\boldsymbol{K}^{(e)}] = \int_{-a}^{a} \int_{-b}^{b} [B_1]^T [\boldsymbol{D}] [B_1] dxdy \tag{26}$$

The $[\boldsymbol{D}]$ matrix appearing in the above equation is an interval matrix owing to the uncertainty of Young's modulus $\boldsymbol{E}$. It can be expressed as follows:

$$[\boldsymbol{D}] = \frac{Eh^3}{12(1-\nu^2)} \begin{bmatrix} 1 & \nu & 0 \\ \nu & 1 & 0 \\ 0 & 0 & \dfrac{(1-\nu)}{2} \end{bmatrix} = \begin{bmatrix} \dfrac{Eh^3}{12(1-\nu^2)} & \dfrac{Eh^3\nu}{12(1-\nu^2)} & 0 \\ \dfrac{Eh^3\nu}{12(1-\nu^2)} & \dfrac{Eh^3}{12(1-\nu^2)} & 0 \\ 0 & 0 & \dfrac{Eh^3}{24(1+\nu)} \end{bmatrix} \tag{27}$$

where $\boldsymbol{E}$ is the interval Young's modulus and ν is the Poisson's ratio.

Following the work of Xiao et.al., (Xiao, Fedele and Muhanna, 2013), the $[\boldsymbol{D}]$ matrix is decomposed as follows:

$$[\boldsymbol{D}] = A_k \, diag(\boldsymbol{\Lambda}_k \boldsymbol{\alpha}_k) A_k^T \tag{28}$$

where $\boldsymbol{\alpha}_k = \boldsymbol{E}$; $\boldsymbol{\Lambda}_k = \left\{ \frac{h^3}{12(1-\nu^2)} \quad \frac{h^3}{12} \quad \frac{h^3}{24(1+\nu)} \right\}^T$; $A_k = \begin{bmatrix} 1 & 0 & 0 \\ \nu & 1 & 0 \\ 0 & 0 & 1 \end{bmatrix}$ (29)

Applying numerical integration to Eq. (26), then

$$\left[\boldsymbol{K}^{(e)}\right] = \sum_{i=1}^{M}\sum_{j=1}^{N} w_i w_j B_1^T(x_i, y_i)\tilde{D}(x_i, y_i)B_1(x_i, y_i) \tag{30}$$

that leads to $$\left[\boldsymbol{K}^{(e)}\right] = \sum_{i=1}^{M}\sum_{j=1}^{N} w_i w_j B_1^T(x_i, y_i)A_k\, diag(\boldsymbol{\Lambda}_k\boldsymbol{\alpha}_k)A_k^T B_1(x_i, y_i) \tag{31}$$

Eq. (31) can be rewritten as

$$\left[\boldsymbol{K}^{(e)}\right] = \begin{bmatrix} B_1^T(x_1, y_1)A_k & B_2^T(x_2, y_2)A_k & \ldots \end{bmatrix} \begin{bmatrix} diag(\boldsymbol{\Lambda}_k\boldsymbol{\alpha}_k(x_1, y_1)) & & \\ & diag(\boldsymbol{\Lambda}_k\boldsymbol{\alpha}_k(x_1, y_1)) & \\ & & \ldots \end{bmatrix} \begin{Bmatrix} A_k^T B_1(x_1, y_1) \\ A_k^T B_1(x_2, y_2) \\ \ldots \end{Bmatrix} \tag{32}$$

So the decomposition for the element stiffness matrix $\left[\boldsymbol{K}^{(e)}\right]$ is expressed as

$$\left[\boldsymbol{K}^{(e)}\right] = \left[A^{(e)}\right] diag(\Lambda\boldsymbol{\alpha}) \left[A^{(e)}\right]^T \tag{33}$$

The stiffness matrix of the structure $\boldsymbol{K}$ is obtained from the element stiffness matrices $\boldsymbol{K}^{(e)}$ described in Eq. (33) as follows:

$$\left[\boldsymbol{K}\right] = \begin{bmatrix} \boldsymbol{K}_1^{(e)} & & & \\ & \boldsymbol{K}_2^{(e)} & & \\ & & \boldsymbol{K}_3^{(e)} & \\ & & & \ldots \end{bmatrix} = \begin{bmatrix} A_1^{(e)} & A_2^{(e)} & A_3^{(e)} & \ldots \end{bmatrix} \begin{bmatrix} diag(\Lambda_1\boldsymbol{\alpha}_1) & & & \\ & diag(\Lambda_2\boldsymbol{\alpha}_2) & & \\ & & diag(\Lambda_3\boldsymbol{\alpha}_3) & \\ & & & \ldots \end{bmatrix} \begin{Bmatrix} A_1^{T(e)} \\ A_2^{T(e)} \\ A_3^{T(e)} \\ \ldots \end{Bmatrix} \tag{34}$$

This can be denoted as

$$\left[\boldsymbol{K}\right] = \left[A\right]\left[\boldsymbol{D}\right]\left[A\right]^T \tag{35}$$

When each plate element is subjected to an interval pressure $\boldsymbol{p}_z$, the corresponding interval force vector $\{\boldsymbol{P}\}$ described in Eq. (23) for the structure can be defined using the M matrix approach outlined by the authors (Muhanna and Mullen, 1999) as follows:

$$\{\boldsymbol{P}\}_{n\times 1} = \begin{Bmatrix} \boldsymbol{P}_1^{(e)} \\ \boldsymbol{P}_2^{(e)} \\ \boldsymbol{P}_3^{(e)} \\ \ldots \end{Bmatrix} = \left[M\right]_{n\times m}\left[\boldsymbol{\delta}\right]_{m\times 1} \tag{36}$$

where n is the number of degrees of freedom for the structure and m is the number of elements. Each column of $[M]$ matrix contains the contribution of deterministic pressure p_z on each plate element and the interval vector $\{\boldsymbol{\delta}\}$ contains interval multipliers corresponding to pressures acting on each of the m elements of the structure. In addition, the vector of point loads acting on the nodes of the structure can be represented as $\{\boldsymbol{P}_c\}$.

The current interval formulation is based on the Element-By-Element (EBE) finite element technique (Muhanna and Mullen, 2001; Rama Rao, Mullen and Muhanna, 2011). In the EBE method, each element has its own set of nodes, but the set of elements is disassembled, so that a node belongs to a single element. A set of additional constraints is introduced to force unknowns associated with coincident nodes to have identical values. Thus, the constraint equation $CU = V$ takes the form

$$[C]\{\boldsymbol{U}\} = 0 \tag{37}$$

where the constraint matrix C is a deterministic one (fixed point matrix). Eq. (17) can be rewritten to represent the interval form of strain-curvature relationship as

$$\{\boldsymbol{\kappa}^{(e)}\} = [B][\Phi]^{-1}\{\boldsymbol{d}\} \tag{38}$$

where $\{\boldsymbol{d}\}$ is the vector of nodal displacements for the element. At the global level, this relation can be expressed as

$$[B_1]\{U\} = \{\boldsymbol{\kappa}\} \tag{39}$$

where $[B_1]$ is the strain-curvature matrix and $\{\boldsymbol{\kappa}\}$ is the vector of interval curvatures for the structure. Eq. (39) can be used as an additional constraint in addition to Eq. (37). Thus the modified potential energy Π^* can be expressed as

$$\Pi^* = \frac{1}{2}\{\boldsymbol{U}\}^T[\boldsymbol{K}]\{\boldsymbol{U}\} - \{\boldsymbol{U}\}^T\{\boldsymbol{P}\} + \lambda_1^T([C]\{\boldsymbol{U}\} - \{V\}) + \lambda_2^T([B_1]\{\boldsymbol{U}\} - \{\boldsymbol{\kappa}\}) \tag{40}$$

Invoking the stationarity of Π^*, that is $\delta\Pi^* = 0$, and considering Eq. (40), we obtain

$$\left(\begin{pmatrix} \boldsymbol{0} & C^T & B_1^T & 0 \\ C & 0 & 0 & 0 \\ B_1 & 0 & 0 & -I \\ 0 & 0 & -I & 0 \end{pmatrix} + \begin{bmatrix} A \\ 0 \\ 0 \\ 0 \end{bmatrix}[\boldsymbol{D}][A \quad 0 \quad 0 \quad 0]\right)\begin{pmatrix} \boldsymbol{U} \\ \boldsymbol{\lambda_1} \\ \boldsymbol{\lambda_2} \\ \kappa \end{pmatrix} = \begin{pmatrix} \boldsymbol{P}_C \\ 0 \\ 0 \\ 0 \end{pmatrix} + \begin{Bmatrix} M \\ 0 \\ 0 \\ 0 \end{Bmatrix}\{\boldsymbol{\delta}\} \tag{41}$$

where λ_1 and λ_2 are vectors of Lagrange Multipliers. The solution of Eq. (41) will provide the values of interval displacements $\boldsymbol{U}$ (primary unknowns) as well as interval values of $\{\boldsymbol{\lambda_1}\}$, $\{\boldsymbol{\lambda_2}\}$ and $\{\boldsymbol{\kappa}\}$ (secondary unknowns) with the same level of sharpness (Rama Rao, Mullen and Muhanna ,2011). It is further observed from Eq. (41) that the Lagrange multipliers $\{\boldsymbol{\lambda_2}\}$ have zero value.

$$\left(\begin{pmatrix} \boldsymbol{0} & C^T & B_1^T & 0 \\ C & 0 & 0 & 0 \\ B_1 & 0 & 0 & -I \\ 0 & 0 & -I & 0 \end{pmatrix}\begin{pmatrix} \boldsymbol{K} & 0 & 0 & 0 \\ 0 & 0 & 0 & 0 \\ 0 & 0 & 0 & 0 \\ 0 & 0 & 0 & 0 \end{pmatrix}\right)\begin{pmatrix} \boldsymbol{U} \\ \boldsymbol{\lambda_1} \\ \boldsymbol{\lambda_2} \\ \boldsymbol{\kappa} \end{pmatrix} = \begin{pmatrix} \boldsymbol{P_C} \\ 0 \\ 0 \\ 0 \end{pmatrix} + \begin{Bmatrix} [M] \\ 0 \\ 0 \\ 0 \end{Bmatrix}\{\boldsymbol{\delta}\} \tag{42}$$

Eq. (41) is now similar to Eq. (3) and thus can be solved using the Neumaier's approach outlined in section 2. The vector of interval moments $\{\boldsymbol{M}\}$ can be obtained from the vector of interval curvatures $\{\boldsymbol{\kappa}\}$ as

$$\begin{Bmatrix} \boldsymbol{M}_x \\ \boldsymbol{M}_y \\ \boldsymbol{M}_{xy} \end{Bmatrix} = [\boldsymbol{D}]\begin{Bmatrix} \boldsymbol{\kappa}_x \\ \boldsymbol{\kappa}_y \\ \boldsymbol{\kappa}_{xy} \end{Bmatrix} = \frac{\boldsymbol{E}h^3}{12(1-\nu^2)}\begin{bmatrix} 1 & \nu & 0 \\ \nu & 1 & 0 \\ 0 & 0 & \dfrac{(1-\nu)}{2} \end{bmatrix}\begin{Bmatrix} \boldsymbol{\kappa}_x \\ \boldsymbol{\kappa}_y \\ \boldsymbol{\kappa}_{xy} \end{Bmatrix} \tag{43}$$

The applicability of the procedure outlined above is illustrated by solving numerical examples in the next section.

5. Example Problems

A thin rectangular plate with clamped edges is chosen to illustrate the applicability of the present approach to handle uncertainty in load and material properties in case of thin plate problems. These examples are chosen to demonstrate the ability of the current approach to obtain sharp bounds to the displacements and forces even in the presence of large number of interval variables. The two example problems are solved for various levels of interval widths of the loads centered at their nominal values. All interval variables are assumed to vary independently. Solution procedure outlined in the previous sections is used to perform the linear interval finite element analysis. The material and geometric properties of the plate are given in Table 1 below. The discretization scheme adopted is shown in Figure 3.

Table 1. Properties of rectangular plate and discretization scheme.

Length Lx	2.0 m
Width Ly	3.0 m
Thickness	0.025 m
Young's modulus	210 GPa
Poisson's ratio ν	0.3
Applied Pressure p_z	14.0×10^3 Pa
Number of divisions along x-axis	nx
Number of divisions along y-axis	ny
Notation for discretization scheme	$nx \times ny$

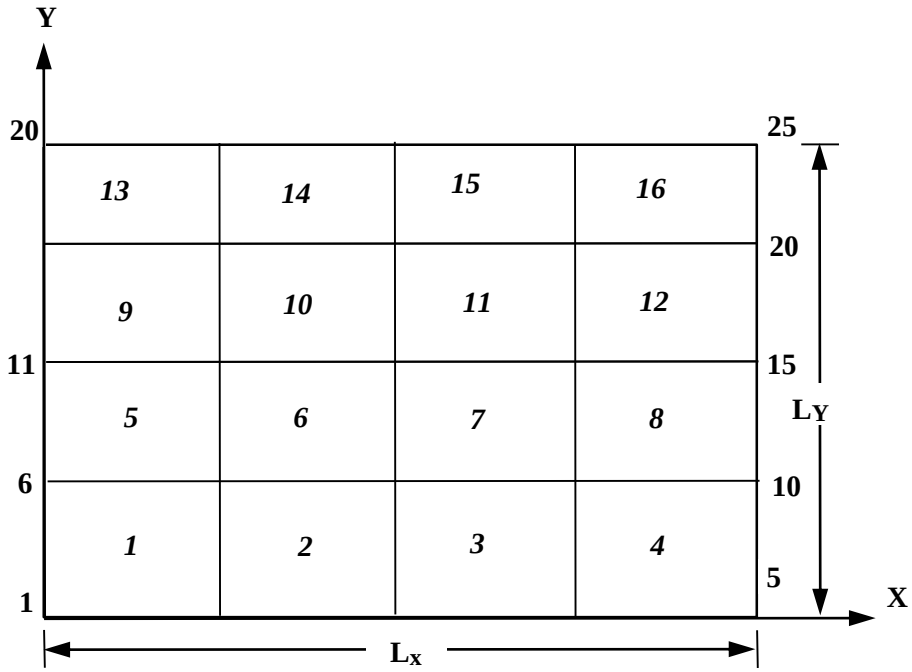

Figure 3. Discretization scheme of rectangular plate.

First the present interval approach is validated by solving the problem of a rectangular plate with a 4x4 discretization scheme. Solution is computed using the present interval approach and combinatorial solution. The computation of results for combinatorial solution required computation of results for 2^{16}=65,536 combinations.

The results obtained for clamped plate for vertical displacement at center of the plate (at node 13), slope θ_y at node 12 and slope θ_x at node 7 at various levels of uncertainty of Young's modulus (E) are shown in Figure 4 , Figure 5 and Figure 6 respectively. Figure 7 and Figure 8 show the variation of M_{xx} and M_{yy} at the center of the plate (at node 13) at various levels of uncertainty of Young's modulus (E). These figures show the lower and upper bounds of the present interval solution and the corresponding results of the combinatorial solution for various levels of uncertainty of Young's modulus from 0 percent to 10 percent. It is observed from these figures that the bounds of the present interval solution sharply enclose the bounds of combinatorial solution at all levels of uncertainty.

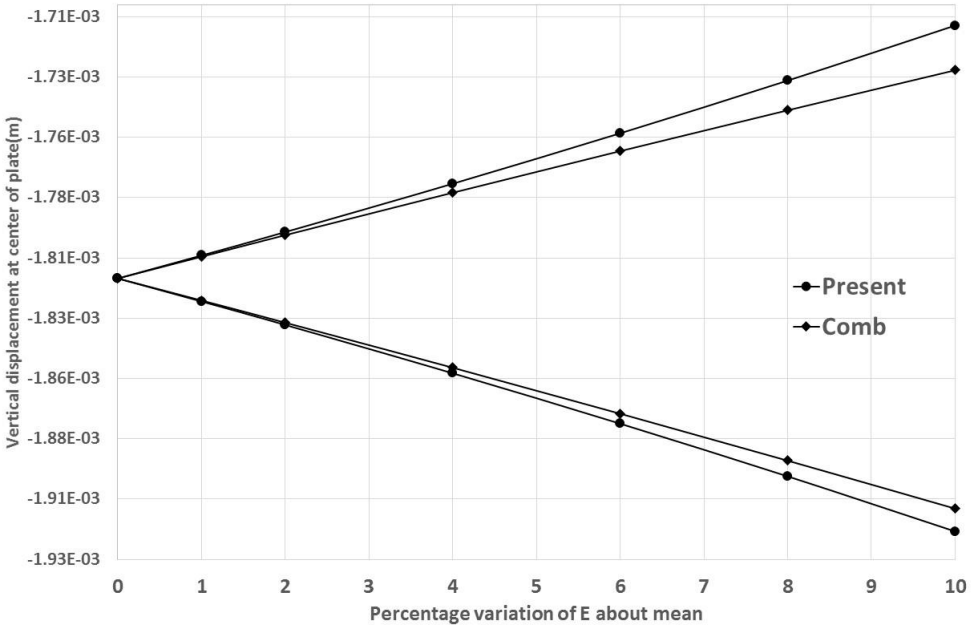

Figure 4. Clamped plate- variation of vertical displacement w_z of center of plate (at node 13) w.r.t. uncertainty of E.

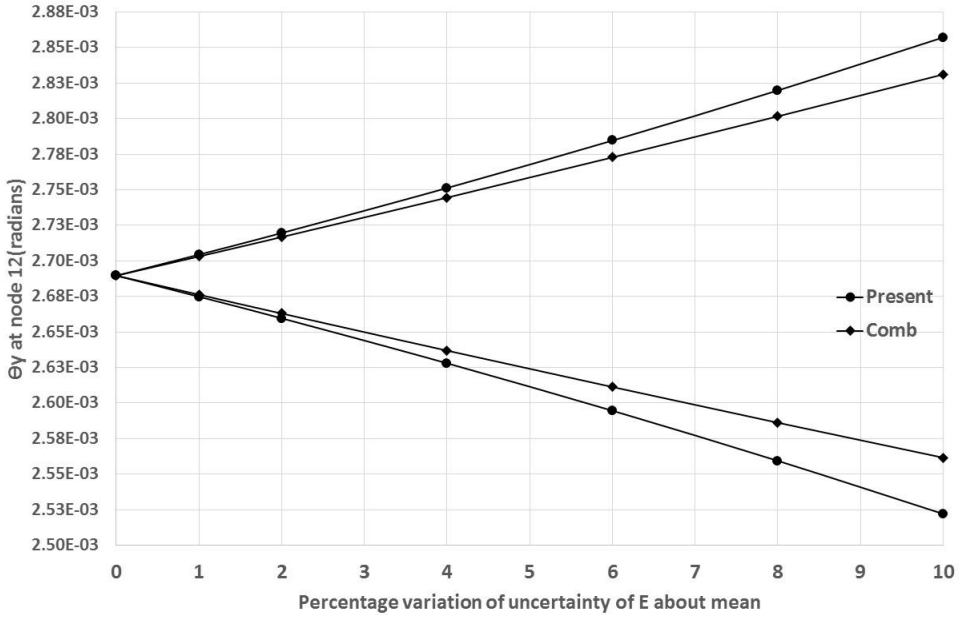

Figure 5. Clamped plate- variation of θ_y at node 12 w.r.t. uncertainty of E.

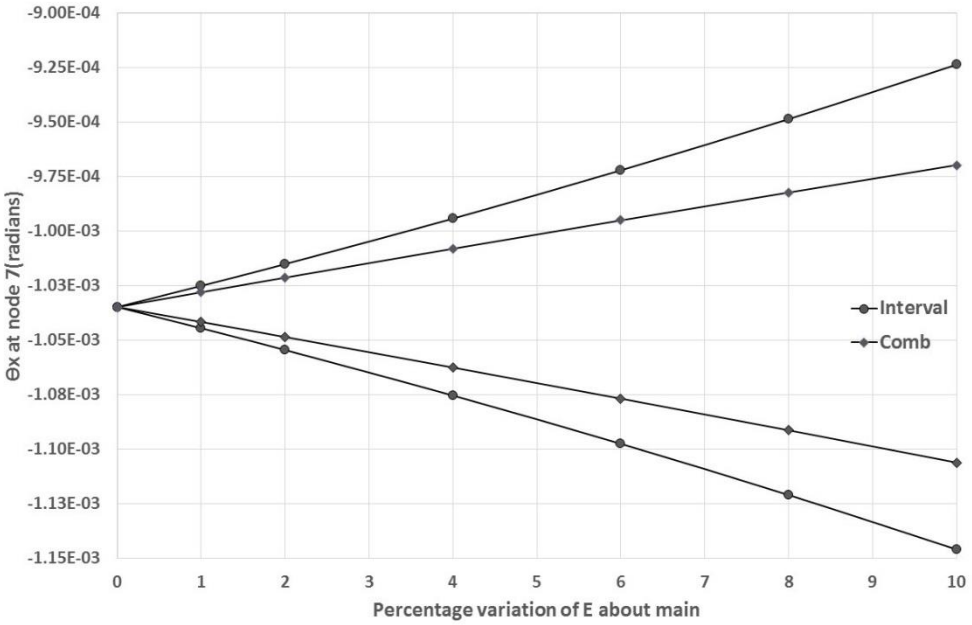

Figure 6. Clamped plate- variation of θ_x at node 7 w.r.t. uncertainty of E.

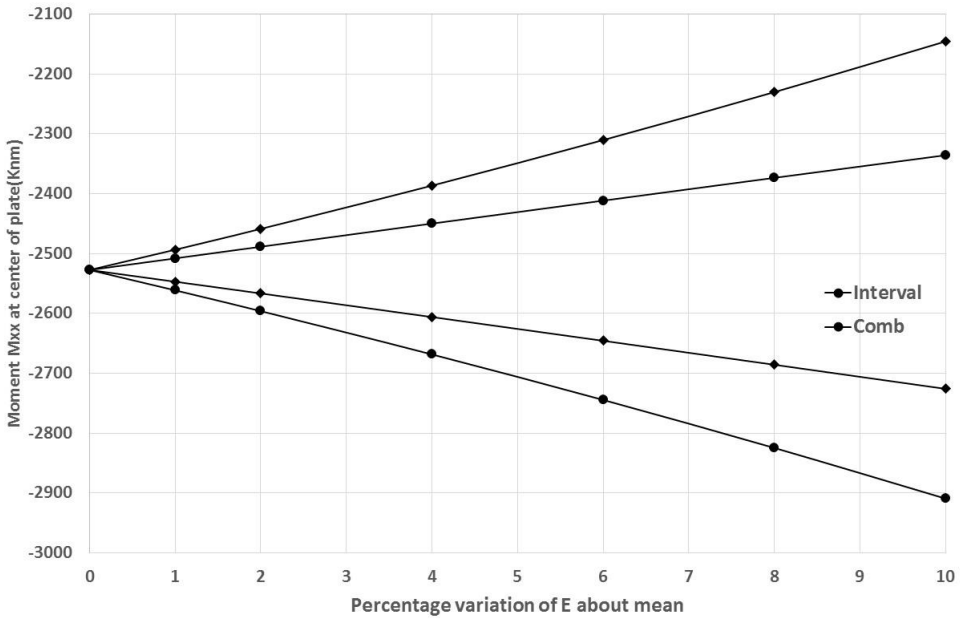

Figure 7. Clamped plate- variation of M_{xx} at center of plate (at node 13) w.r.t. uncertainty of E.

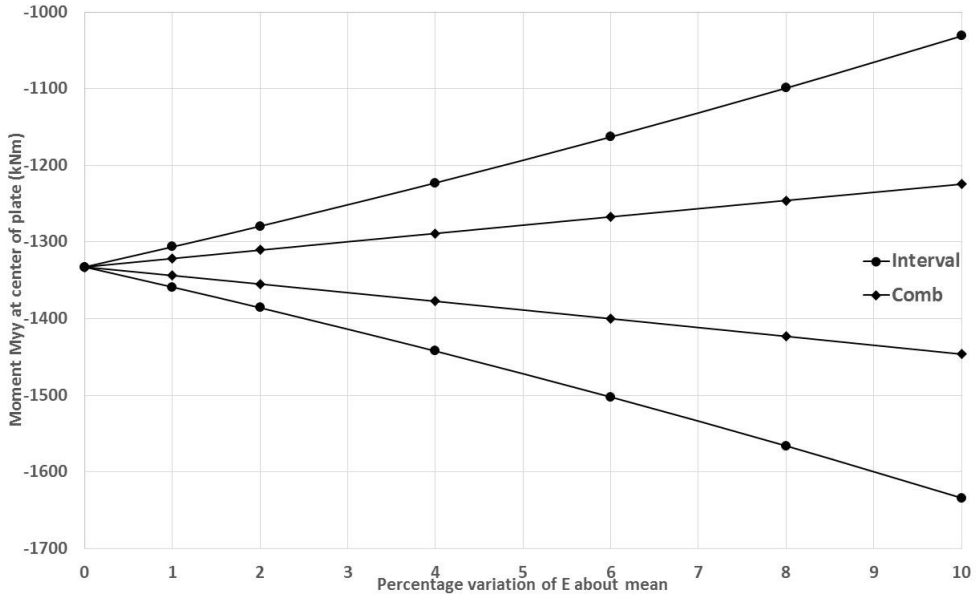

Figure 8. Clamped plate- variation of M_{yy} at center of plate (at node 13) w.r.t. uncertainty of E.

Results are computed for the 4×4 plate for the following cases:

A) Load uncertainty of 10 percent (±5 percent variation of load about its mean value) alone is present
B) 1 percent uncertainty of E(±0.5 percent variation of E about its mean value) alone
C) Load uncertainty of 10 percent along with 1 percent uncertainty of E.

Tables 2, 3 and 4 present the results of selected displacements and rotations corresponding to cases A, B and C respectively. Similarly, Tables 5, 6 and 7 present the results of moments at the center of the plate corresponding to cases A, B and C respectively.

It is observed from the Tables 2 and 5 that the results of the interval solution coincide with those obtained using combinatorial approach and thus provide exact bounds to the combinatorial solution. It is observed from Tables 3 and 6 that the interval solution gives sharp bounds to the values of selected displacements and rotations w.r.t the corresponding values obtained using combinatorial solution. As already mentioned, these solutions required computation of 2^{16} =65536 combinations. Tables 4 and 7 show the results computed for 10 percent load uncertainty along with 1 percent uncertainty of Young's modulus E. It is impractical to compute combinatorial solution in this case, as it would require computation of solution for $2^{16}\times2^{16}$=4,294,967,296 combinations. Instead, the bounds of the solution are computed using MCS (Monte-Carlo Simulations). The results computed in Tables 4 and 7 are for 20,000 simulations. It is to be noted here that the results obtained using MCS provide inner bounds to the combinatorial solution whereas the results obtained using interval solution provide outer bounds to the combinatorial solution.

Table 2. Clamped rectangular plate (4×4)– selected displacements and rotations of the plate for 10% uncertainty of load (Case-A).

Method	$w_{13}\times10^3$(m)		$\theta_x \times10^3$(radians) at node 7		$\theta_y \times10^3$(radians) at node 12	
	Lower	Upper	Lower	Upper	Lower	Upper
Combinatorial	-1.90416	-1.72281	-1.10534	-0.96432	2.55516	2.82412
Interval	-1.90416	-1.72281	-1.10534	-0.96432	2.55516	2.82412
Error%	0.0	0.0	0.0	0.0	0.0	0.0

Table 3. Clamped rectangular plate(4×4)- selected displacements and rotations of the plate for 1% uncertainty of E (Case-B).

Method	$w_{13}\times10^3$(m)		$\theta_x \times10^3$(radians) at node 7		$\theta_y \times10^3$(radians) at node 12	
	Lower	Upper	Lower	Upper	Lower	Upper
Combinatorial	-1.82260	-1.80446	-1.04167	-1.02805	2.67626	2.70315
Interval	-1.82302	-1.80395	-1.04455	-1.02510	2.67482	2.70446
Error%	0.023	0.028	0.276	0.287	0.054	0.048

Table 4. Clamped rectangular plate(4×4)- selected displacements and rotations of the plate for 10% uncertainty of load and 1% uncertainty of E (Case–C).

Method	$w_{13}\times10^3$(m)		$\theta_x \times10^3$(radians) at node 7		$\theta_y \times10^3$(radians) at node 12	
	Lower	Upper	Lower	Upper	Lower	Upper
MCS	-1.87530	-1.74648	-1.07575	-0.97905	2.59554	2.78867
Interval	-1.91180	-1.71030	-1.10937	-0.94955	2.54020	2.84412
Error%	1.946	2.072	3.125	3.013	2.132	1.988

Table 5. Clamped rectangular plate (4×4)- moments at the center of the plate for 10% uncertainty of load (Case-A).

Method	M_{xx} (kN) at node 13		$M_{yy} \times10^3$(kN) at node 13	
	Lower	Upper	Lower	Upper
Comb	-2653.612	-2400.887	-1421.684	-1243.397
Interval	-2653.612	-2400.887	-1421.684	-1243.397
Error%	0.0	0.0	0.0	0.0

Table 6. Clamped rectangular plate (4×4)- moments at the center of the plate for 1% uncertainty of E (Case-B).

Method	M_{xx} (kN) at node 13		$M_{yy} \times10^3$(kN) at node 13	
	Lower	Upper	Lower	Upper
Comb	-2546.794	-2507.773	-1343.636	-1321.502
Interval	-2561.199	-2493.300	-1358.769	-1306.311
Error%	0.566	0.577	1.126	1.150

Table 7. Clamped rectangular plate (4×4)- moments at the center of the plate for 10% uncertainty of load and 1% uncertainty of E (Case-C).

Method	M_{xx} (kN) at node 13		M_{yy} ×10^3(kN) at node 13	
	Lower	Upper	Lower	Upper
MCS	-2612.438	-2425.942	-1383.487	-1259.684
Interval	-2678.945	-2358.225	-1434.310	-1211.391
Error%	2.546	2.791	3.674	3.834

Figure 9 presents the variation of the lower and upper bounds of the interval displacement w_z along the length and width of the plate respectively. Figure 10 presents the variation of the lower and upper bounds of the slope θ_x along the width of the plate. Figure 11 presents the variation of the lower and upper bounds of the slope θ_y along the length of the plate.

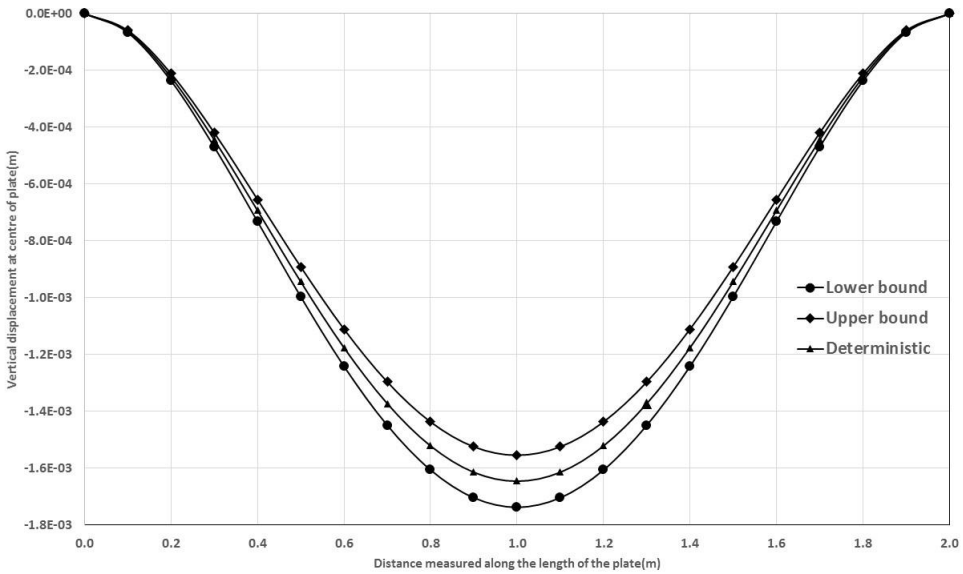

Figure 9. Clamped plate- variation of vertical displacement along the length of the plate with 10% uncertainty of load and 1% uncertainty of E.

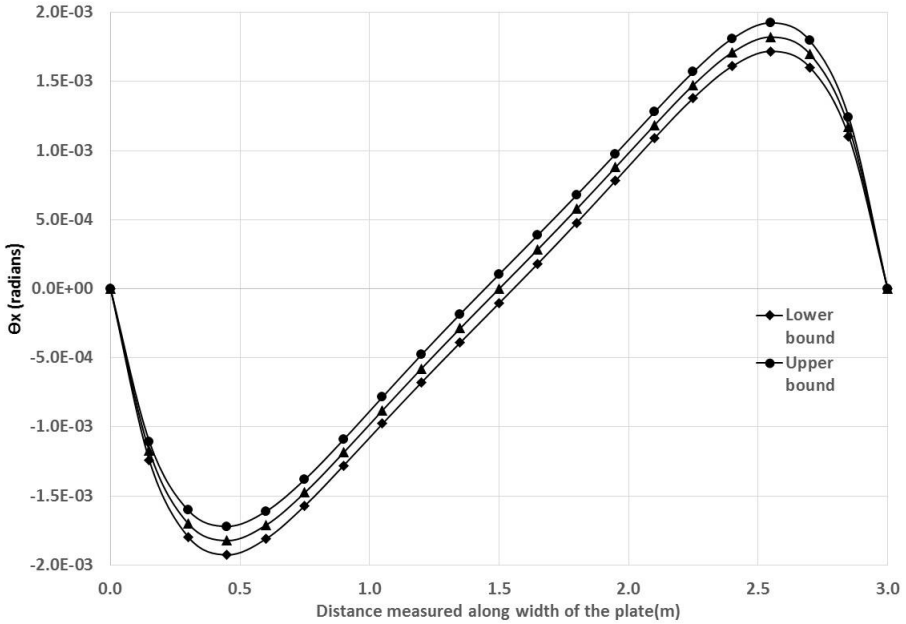

Figure 10. Clamped plate- variation of θ_x along the width of the plate with 10% uncertainty of load and 1% uncertainty of E.

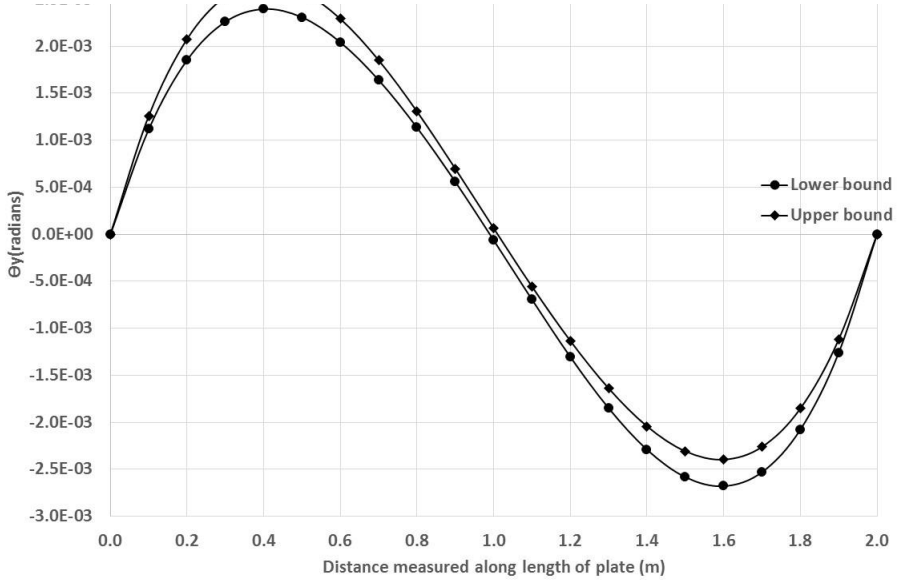

Figure 11. Clamped plate- variation of θ_y along the length of the plate with 10% uncertainty of load and 1% uncertainty of E.

Tables 8, 9 and 10 present the values of selected displacements and rotations for a discretization scheme of 20×20 (400 elements) for cases A, B and C respectively. Similarly, Tables 11, 12 and 13 present the values of moments at the center of the plate for cases A, B and C respectively. It is to be noted here that the computation of combinatorial solution for cases A or B would require 2^{400} combinations while it would require computation of 2^{800} combinations for case C. Thus it is practically impossible for to compute the combinatorial solution. Instead, the results of the bounds obtained using 10000 Monte Carlo simulations are presented. It is here to be noted that the bounds of the interval solution enclose the corresponding bounds of the combinatorial solution from outside. On the other hand, the bounds of the results computed using Monte Carlo solution enclose the corresponding bounds of combinatorial solution from inside. It is to be further noted that the percentage error reported in Tables 5 *through* 13 can be reduced by increasing the number of simulations. However it is observed that it is computationally time consuming.

Table 8. Clamped rectangular plate (20×20)– displacements at the center of the plate for 10% uncertainty of load (Case-A).

Method	$w_{221}\times10^3$(m)		$\theta_x\times10^3$(radians) at node 111		$\theta_y\times10^3$(radians) at node 216	
	Lower	Upper	Lower	Upper	Lower	Upper
MCS	-1.65855	-1.63336	-8.43218	-8.25503	2.42576	2.46399
Interval	-1.72747	-1.56295	-8.85896	-7.81985	2.32204	2.56667
Error%	4.155	4.311	5.061	5.272	4.276	4.167

Table 9. Clamped rectangular plate (20×20)– displacements center of the plate for 1% uncertainty of E (Case-B).

Method	$w_{221}\times10^3$(m)		$\theta_x\times10^4$(radians) at node 111		$\theta_y\times10^3$(radians) at node 216	
	Lower	Upper	Lower	Upper	Lower	Upper
MCS	-1.64694	-1.64384	-8.35812	-8.32283	2.44201	2.44683
Interval	-1.65386	-1.63656	-8.42754	-8.25127	2.43025	2.45845
Error%	0.420	0.443	0.831	0.860	0.482	0.475

Table 10. Clamped rectangular plate (20×20)– displacements at the center of the plate for 10% uncertainty of load and 1% uncertainty of E (Case-C).

Method	$w_{221}\times10^3$(m)		$\theta_x\times10^3$(radians) at node 111		$\theta_y\times10^3$(radians) at node 216	
	Lower	Upper	Lower	Upper	Lower	Upper
MCS	-1.66052	-1.63068	-8.43013	-8.25141	2.42244	2.46768
Interval	-1.73665	-1.55377	-8.95341	-7.72540	2.30699	2.58172
Error%	4.585	4.716	6.207	6.375	4.766	4.621

Table 11. Clamped rectangular plate (20×20)– moments center of the plate for 10% uncertainty of load (Case-A).

Method	M_{xx} (kN) at node 221		$M_{yy}\times10^3$(kN) at node 221	
	Lower	Upper	Lower	Upper
MCS	-2096.211	-2057.435	-1154.767	-1124.961
Interval	-2180.916	-1973.210	-1204.756	-1077.381
Error%	4.041	4.094	4.329	4.229

Table 12. Clamped rectangular plate (20×20)– moments at the center of the plate for 1% uncertainty of E (Case-B).

Method	M_{xx} (kN) at node 221		$M_{yy} \times 10^3$(kN) at node 221	
	Lower	Upper	Lower	Upper
MCS	-2088.860	-2064.535	-1146.630	-1135.780
Interval	-2127.365	-2026.761	-1175.676	-1106.461
Error%	1.843	1.830	2.533	2.581

Table 13. Clamped rectangular plate (20×20)– moments at the center of the plate for 10% uncertainty of load and 1% uncertainty of E (Case-C).

Method	M_{xx} (kN) at node 221		$M_{yy} \times 10^3$(kN) at node 221	
	Lower	Upper	Lower	Upper
MCS	-2108.068	-2051.424	-1161.423	-1121.883
Interval	-2234.305	-1919.821	-1242.057	-1040.080
Error%	5.988	6.415	6.943	7.292

6. Conclusion

A linear Interval Finite Element Method (IFEM) for structural analysis of thin plates is presented. Uncertainty in the applied load and Young's modulus is represented as interval numbers. Results are also computed using combinatorial solution and Monte Carlo simulations as appropriate. Example problems illustrate the applicability of the present approach to the problem of predicting the structural behavior of thin plates in the presence of uncertainties.

Acknowledgements

The first author would like to gratefully acknowledge the help received via international travel funding by the Technical Education Quality Improvement Program (TEQIP- Phase II) of Government of India and its sanction by the administration of Vasavi College of Engineering, Hyderabad, India.

References

Bathe, K. Finite Element Procedures, Prentice Hall, Englewood Cliffs, New Jersey 07632, New Jersey, 1996.

Batista, M. Uniformly Loaded Rectangular Thin Plates with Symmetrical Boundary Conditions. Cornel University Library, USA, http://arxiv.org/abs/1001.3016,2010.

Dessombz, O., F. Thouverez, J.-P. Laîné, and L. Jézéquel. Analysis of mechanical systems using interval computations applied to finite elements methods. *J. Sound. Vib.*, 238(5):949-968, 2001.

Gallagher, R. H. Finite Element Analysis Fundamentals, Prentice Hall, Englewood Cliffs, USA, 1975.

Knüppel,O. PROFIL / BIAS — A Fast Interval Library. Computing, 53:277–287, 1994.

Köylüoglu, U., S. Cakmak, N. Ahmet and R. K. Soren. Interval Algebra to Deal with Pattern Loading and Structural Uncertainty. *Journal of Engineering Mechanics* 121(11): 1149–1157, 1995.

Lim, C.W., S. Cui, W. A. Yao. On new symplectic elasticity approach for exact bending solutions of rectangular thin plates with two opposite sides simply supported, International Journal of Solids and Structures, Volume 44(16):5396-5411, 2007.

Moore, R., E. Interval Analysis, Prentice-Hall, Englewood Cliffs, N.J., 1966.

Moore, R. E. *Methods and applications of interval analysis*, SIAM, Philadelphia, 1979.

Moore, R. E., R. B. Kearfott, M. J. Cloud. Introduction to Interval analysis, SIAM, 2009.

Muhanna, R. L. and R. L. Mullen. Development of Interval Based Methods for Fuzziness in Continuum Mechanics. In Proceedings of *ISUMA-NAFIPS'95*: *17-20 September, IEEE, 1995*.

Muhanna, R. L. and R. L. Mullen. Uncertainty in Mechanics Problems—Interval-Based Approach, *Journal of Engineering Mechanics* 127(6): 557–566, 2001.

Muhanna, R. L., H. Zhang and R. L. Mullen. Interval finite element as a basis for generalized models of uncertainty in engineering mechanics. *Reliable Computing*, 13(2):173–194, 2007.

Nakagiri, S. and N. Yoshikawa. Finite Element Interval Estimation by Convex Model. *In Proceedings of 7th ASCE EMD/STD Joint Specialty Conference on Probabilistic Mechanics and Structural Reliability, WPI, MA, 7.-9. August, 1996.*

Neumaier, A. *Interval methods for systems of equations*, Cambridge University Press, 1990.

Neumaier, A. and A. Pownuk. Linear Systems with Large Uncertainties, with Applications to Truss Structures, *Reliable Computing*, 13(2):149-172, 2007.

Pownuk, A. Efficient method of solution of large scale engineering problems with interval parameters." *Proc. NSF workshop on reliable engineering computing* (REC2004), R. L. Muhanna and R. L. Mullen, eds., Savannah, GA, USA, 2004.

Rama Rao, M. V., R. L. Mullen, R. L. Muhanna. A New Interval Finite Element Formulation with the Same Accuracy in Primary and Derived Variables, International Journal of Reliability and Safety, Vol. 5, Nos. ¾, 2011.

Rao, S. S. and P. Sawyer. Fuzzy finite element approach for analysis of imprecisely defined systems. *AIAA J.*, 33(12):2364–2370, 1995.

Rao, S. S. and L. Berke. Analysis of uncertain structural systems using interval analysis. *AIAA J.*, 35(4):727–735, 1997.

Rao, S. S. and Li Chen. Numerical solution of fuzzy linear equations in engineering analysis. *International Journal of Numerical Methods in Engineering.*,43:391–408, 1998.

Reddy, J.N. *Theory and Analysis of Elastic Plates and Shells*. Second edition. CRC Press. Taylor and Francis group, Boca Raton, London and New York, 2007.

Rump, S.M. INTLAB - INTerval LABoratory. In Tibor Csendes, editor, Developments in Reliable Computing, pages 77-104. Kluwer Academic Publishers, Dordrecht, 1999.

Sun microsystems. *Interval arithmetic in high performance technical computing*. Sun microsystems. (A White Paper), 2002.

Szilard, R. *Theories and Applications of Plate Analysis: Classical Numerical and Engineering Methods*, 2004.

Wiley Timoshenko, S. and S. Woinowsky-Krieger. *Theory of Plates and Shells.* Second edition. McGraw Hill, 1959.

Xiao, N., F. Fedele and R. L. Muhanna. *Inverse Problems Under Uncertainties-An Interval Solution for the Beam Finite Element*, in Deodatis, B. R. Ellingwood, D. M. Frangopol, Icossar, ISBN: 978-1-138-00086-5, 2013.

Zhang, H. Nondeterministic Linear Static Finite Element Analysis: An Interval Approach. *Ph.D. Dissertation, Georgia Institute of Technology, School of Civil and Environmental Engineering*, 2005.